High power λ ~ 8.5 μm quantum cascade laser grown by MOCVD operating continuous-wave up to 408 K

Teng Fei[1,2], Shenqiang Zhai[1, †], Jinchuan Zhang[1], Ning Zhuo[1], Junqi Liu[1,2], Lijun Wang[1,2], Shuman Liu[1], Zhiwei Jia[1], Kun Li[1, 2], Yongqiang Sun[1, 2], Kai Guo[1], Fengqi Liu[1, 2, †] and Zhanguo Wang[1,2]

[1]Key Laboratory of Semiconductor Materials Science, Institute of Semiconductors, Chinese Academy of Sciences, Beijing Key Laboratory of Low Dimensional Semiconductor Materials and Devices, Beijing 100083, China

[2]Center of Materials Science and Optoelectronics Engineering, University of Chinese Academy of Sciences, Beijing 100049, China

† Corresponding author. Email: zsqlzsmbj@semi.ac.cn, fqliu@semi.ac.cn

Abstract: Quantum cascade laser (QCL) enduring high temperature continuous-wave (CW) operation is of paramount importance to address their application in gas sensing. We report on the realization of lattice-matched InGaAs/InAlAs/InP QCL materials grown by metal-organic chemical vapor deposition (MOCVD). High-quality interface structure designed for light emission at 8.5 μm was achieved by optimizing and precise controlling of growth conditions. A CW output power of 1.04 W at 288 K was obtained from a 4 mm-long and 10 μm-wide coated laser. Corresponding maximum wall-plug efficiency and threshold current density were 7.1% and 1.18 kA/cm^2. The device can operate in CW mode up to 408 K with an output power of 160 mW, which demonstrates excellent temperature stability.

Keywords: Quantum cascade laser; Metal-organic chemical vapor deposition; Continuous-wave; Interface roughness

PACS: 85.40.-e **EEACC:** 2560; 2560B

1. Introduction

Quantum cascade lasers (QCLs)[1] are compact and powerful light sources covering mid-infrared (MIR) to terahertz regimes. Based on the cascaded intersubband transitions, QCLs have been applied in various scientific and industrial applications, such as optical frequency comb[2] and gas sensing[3]. High power continuous-wave (CW) operation QCLs are strongly needed to achieve long-distance sensing and communication. Since the first realization of QCL in 1994, novel designs such as bound-to-continuum[4] (BTC) and double-phonon resonance[5] (DPR) have been raised to realize high-performance QCLs. Molecular beam epitaxy (MBE) has been widely used to grow the active core of QCLs, because of two main features: sharp interfaces and precise control of layer thickness. However, for the reason of high vacuum operating processes, MBE technique bears low QCL production capacity and high QCL cost. Another competitive counterpart technique, metal-organic chemical vapor deposition (MOCVD), has been used for growing high quality QCL wafers with high yield. Several groups have reported high-performance CW operated QCLs grown by MOCVD. Watt-level room temperature CW output power of InGaAs/InAlAs material system using multi-

composition QCL emitting at λ ~ 8 μm[6], lattice-matched QCL emitting at λ ~ 9 μm[7], and strain-balanced QCL emitting at λ ~ 10 μm[8] have been reported. By taking into account the effect of interface grading, which is a fundamental phenomenon in MOCVD-grown materials, Wang et al redesigned the band structures and realized high-performance QCLs emitting from 7.5 μm to 8.5 μm[9].

Despite the aforementioned achievements, MOCVD-grown QCLs possess three drawbacks: (I) in the long-wave infrared (LWIR, 8–12 μm) region, the maximum WPE of room temperature CW operating QCL is no more than 7%, which is much less than that of MBE-grown QCLs[10, 11]. (II) Although the room temperature CW output power of MOCVD-grown QCLs in LWIR region can reach 1 W, the power drops rapidly when temperature increases. (III) Compared with MBE-grown QCLs, the MOCVD-grown QCLs show relatively larger threshold current density. All three presented points mainly root in interface roughness (IFR). In fact, MOCVD is based on complicated gas sources reactions in a low-pressure condition, which results in much longer gas residence time compared with MBE. The hetero-interfaces of InGaAs/InAlAs are unavoidable graded[9], which leads to enhanced IFR. As a result, the optical loss and threshold current density of MOCVD-grown devices are generally higher[12, 13]. This effect is more severe in LWIR due to the diagonal nature of the laser transition, thereby hindering the improvement of power efficiency and working temperature of MOCVD-grown QCLs[14]. Therefore, the interface quality of QCL active region becomes crucial.

In this letter, we report the demonstration of high-performance QCLs grown by MOCVD. By optimizing and precise controlling of growth conditions, high-quality interface lattice-matched InGaAs/InAlAs/InP QCL structure is obtained. Watt-level room temperature CW operated devices emitting at λ ~ 8.5 μm give wall-plug efficiency higher than all these previously reported results. Furthermore, the devices are robust, proved by the output power as high as 160 mW in CW mode at 408 K.

2. Material growth and characterization

The structures were fully grown using a low-pressure MOCVD with a close-coupled showerhead reactor. We first grew 1 μm-thick $In_{0.53}Ga_{0.47}As$ and $In_{0.52}Al_{0.48}As$ bulk materials by varying the growth temperature and V/III ratios from 600 ℃ to 700 ℃ and 15 to 200 respectively. The optimal ranges were determined based on the background doping and electron mobility obtained from Hall measurement and the surface morphorgy obtained using atomic force microscopy (AFM). Fig.1 shows the surface images of lattice-matched $In_{0.53}Ga_{0.47}As$ (left) and $In_{0.52}Al_{0.48}As$ (right) layers measured by AFM. Step-flow mode can be observed, indicating good surface morphology. The morphology of InAlAs shows moderate degradation, which is reasonable due to the low migration rate of Al atoms. Precise control over the layer thicknesses and compositions were ensured using process calibration with the combination of optical in-situ and ex-situ techniques, such as scanning electron microscopy (SEM) and high resolution X-ray diffraction (XRD). Then the QCL superlattice was grown to specify growth conditions. Considering the relatively large allowance for structure fluctuations, single phonon resonance-continuum depopulation QCL structure was adopted[15]. For the reason of high growth temperature, the crystal quality of MOCVD-grown QCL is no longer an issue. The main detrimental factor is the interface roughness. Iterative optimized experiments of growth conditions including growth temperature, growth rates, V/III ratios, and growth interrupts between $In_{0.53}Ga_{0.47}As$ and $In_{0.52}Al_{0.48}As$ interfaces have been conducted to achieve high-quality interface.

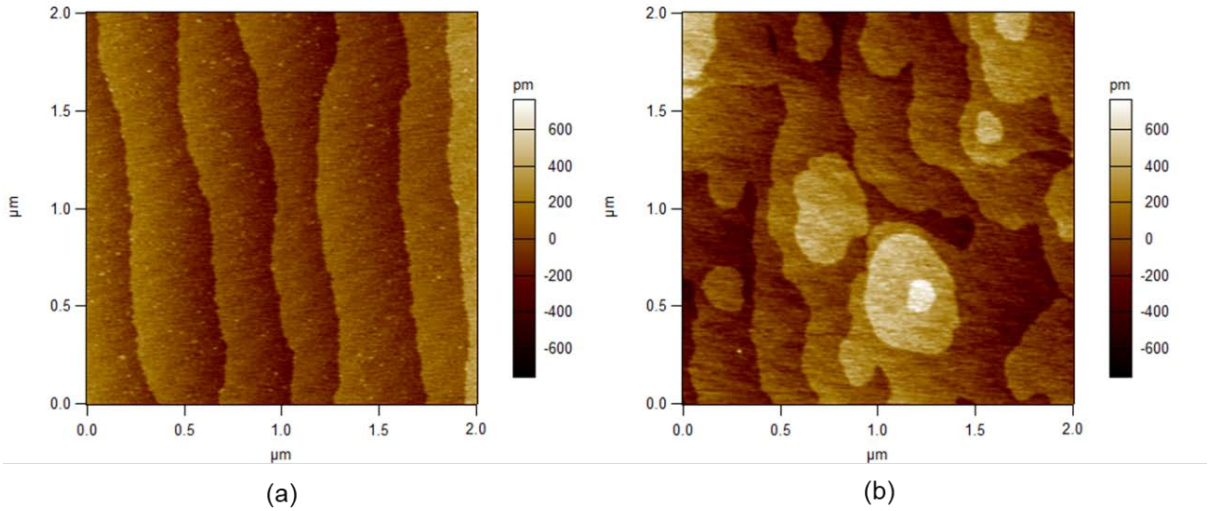

Fig. 1. AFM images (2 × 2 μm^2) of lattice-matched of (a) InGaAs and (b) InAlAs in contact mode.

The QCL structure similar to Ref [9] was fully grown on highly doped InP substrate (2 × 10^{18} cm^{-3}). The layer thicknesses in nanometers, starting from the first injection barrier, are as follows: **4.0**/1.3/**1.0**/5.2/**0.9**/5.1/**1.0**/4.7/**1.6**/3.6/**2.2**/2.9/**1.8**/2.7/**1.9**/2.6/**2.0**/2.4/**2.5**/2.5/**3.1**/2.3, where the bold numbers represent the InAlAs barrier, and the underlined layer is doped with a concentration of 2 × 10^{17} cm^{-3}. The epitaxial layer sequence starting from the InP substrate is as follows: 0.5 μm InP buffer layer(1 × 10^{17} cm^{-3}), 3 μm low-doped InP cladding layer (4 × 10^{16} cm^{-3}), 300 nm InGaAs confinement layer (5 × $10^{16}$$cm^{-3}$), 35 periods InGaAs-InAlAs active structure, 300 nm InGaAs confinement layer (5 × 10^{16} cm^{-3}), 3.3 μm low-doped InP cladding layer (4 × 10^{16} cm^{-3}), 0.4 μm graded-doped InP layer (from 1 × 10^{17} cm^{-3} to 1×$10^{18}$$cm^{-3}$), and 0.3 μm InP contact layer (5 × 10^{18} cm^{-3}). Here we choose the thicknesses of InGaAs confinement layers to be 300 nm to reduce thermal accumulation. The simulation[16] showed that reducing the thickness of the InGaAs confinement layer could remove heat efficiently with the small penalty to confinement factor (Γ).

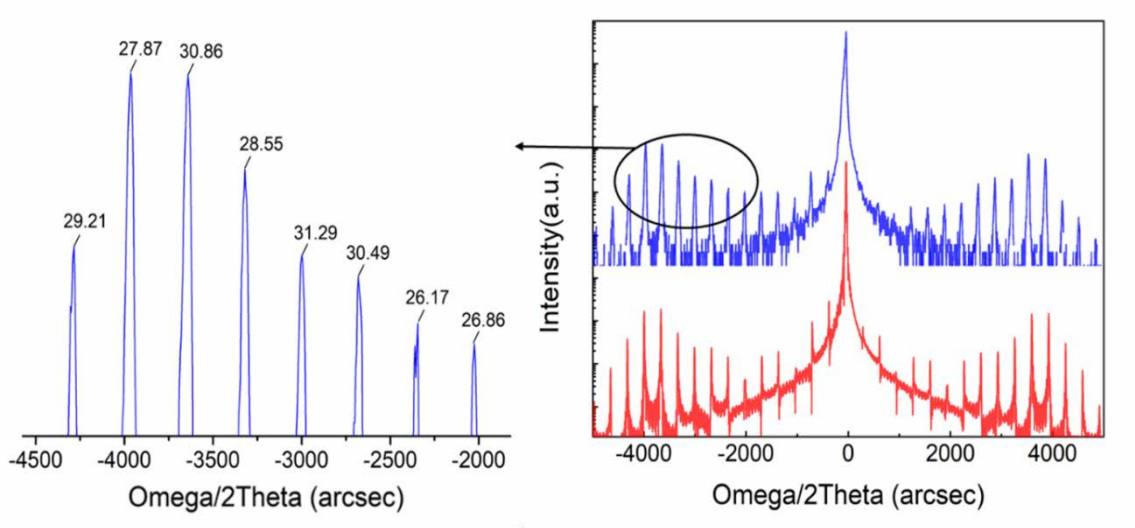

Fig. 2. The right panel shows high-resolution XRD of experimental (blue, upper curve) and simulated (red, lower curve) results of lattice-matched QCL structures. The left shows the partially enlarged view of satellite peaks above, labeled the FWHM in arc seconds.

Fig.2 (right) compares the measured and simulated high-resolution XRD results. Experimental result is almost fully in line with the simulated one. Fig.2 (left) shows the enlarged view of satellite

peaks with full width at half maximum (FWHM) labeled, which are given by fitting the peaks with a Gaussian distribution. Multiple high-order satellite peaks can be clearly observed with extremely sharp and narrow FWHM of about 30 arc seconds. In order to achieve smooth interfaces, it is crucial to have a reliable means of determining the IFR in the grown structures. A number of characterization techniques including transmission electron microscopy (TEM) have been used[17], but we utilized high-resolution XRD to characterize the QCL structures[18] considering its practicality. The observation of multiple satellite peaks in the X-ray pattern is considered as a criterion for evaluating a high-quality hetero-interface which indicates excellent in-plane homogeneity in terms of layer thickness and chemical composition[19]. According to the kinematic theory of X-ray diffraction, the FWHM of the *n*th satellite peak is strongly related to IFR[20]. Note that the FWHM values of MOCVD-grown QCLs is comparable with those of MBE-grown QCLs of similar lattice-matched QCL structures in our laboratory[3]. This indicates that the QCLs grown by MOCVD have similar interfacial quality compared to MBE, which is well known for its excellent interfacial control. The above narrow satellite peaks suggest small IFR, which guarantee the high performance of QCLs. Although other groups have reported watt-level MOCVD grown QCLs, no credible narrow satellite are presented. MIT Lincoln Laboratory have struggled for MOCVD-grown QCL many years and achieved a series of prominent results. But the reported FWHM of satellite peaks in lattice-matched InGaAs/InAlAs superlattice is larger than 40 arc seconds[9].

3. Device performance

The fabrication process of QCLs is as follows. The wafer was processed into a buried heterostructure (BH) configuration with a ridge width of 10 μm. Firstly, the wafer was patterned into stripes along with [110] direction by using a 300 nm-thick SiO_2 mask and wet-etched through the active region into a double-channel geometry. After etching and rinsing, Fe-doped semi-insulating InP was selective-area regrown by MOCVD to planarize the channels. Then SiO_2 mask was removed, and a new 300 nm-thick SiO_2 layer was deposited by PECVD as an electrical isolation layer. The current injection windows were opened on the top of the ridge by lithography and HF etching. Besides, top contact was made, including a Ti/Au layer by e-beam evaporation and a 5 μm-thick Au layer by electroplating. After the wafer was thinned down to 120 μm and polished, an AuGeNi/Au layer was evaporated as the bottom contact. Finally, the processed wafer was cleaved into 4 mm bars, and a high-reflectivity coating consisting of Al_2O_3/Ti/Au/Ti/Al_2O_3 (200/10/100/10/120 nm) was applied on the back facet with the front facet left uncoated. For packaging, the chips were soldered epi-down on diamond submounts to improve heat removal efficiency. Then the submounts with chips were mounted on the copper heat sinks with indium solder followed by wire bonding.

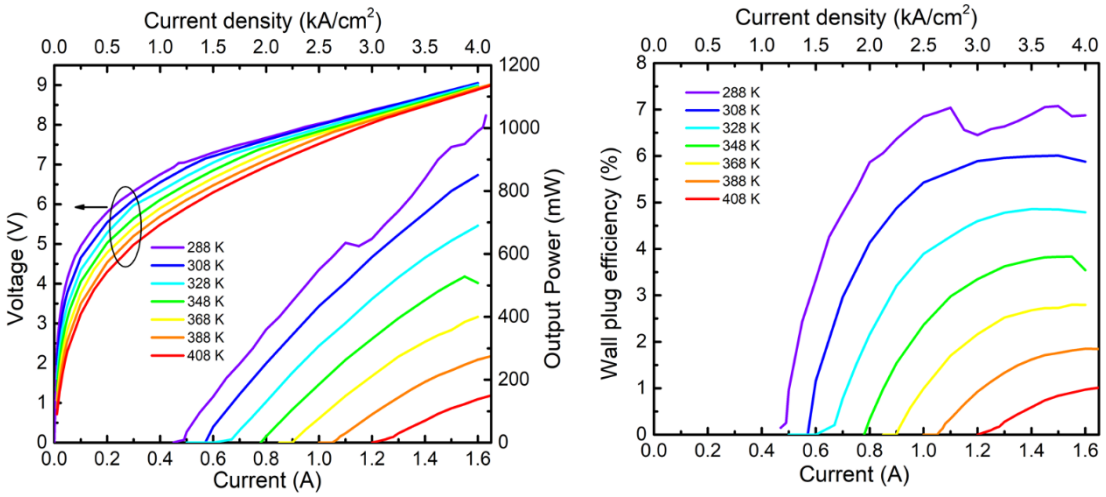

Fig. 3. (a) Power-current-voltage relations of 10 μm × 4 mm-long, and HR coated laser at different temperatures in CW condition. (b) Wall plug efficiency verse current injection characteristics at different temperatures

Fig.3 (a) shows CW power and applied voltage verse current (PIV) curve at different temperatures. The CW optical power was measured by fixing a laser on the water-cooling platform with a chip facet close to a calibrated thermopile detector. The temperature was monitored by a thermistor and controlled by a thermoelectric cooler (TEC). A total amount of 1.04 W CW output power was obtained at 288 K, with a threshold current density of 1.18 kA/cm^2. Fig.3 (b) shows the calculated wall-plug efficiency versus injection current at different temperatures. The maximum WPE is 7.1% at 288 K, which higher than all previously published results obtained from MOCVD-grown LWIR QCLs. In addition, the threshold current density presented here is among the lowest (1.5 kA/cm^2 in Ref [10, 11], 1.6 kA/cm^2 in Ref [6], and 2.5 kA/cm^2 in Ref [21]) when compared with other high-power (watt-level) LWIR QCLs.

Besides relatively high efficiency and low threshould current density, a remarkable feature is that QCLs work up to 408 K in CW mode with the output power of 160 mW and the WPE of 1%. This distinctive feature gives the direct evidence that the QCLs are robust. CW operation in high temperature is difficult to achieve given by the natural cascade characteristic of QCLs. A dedicated effort has been put from the perspective of the active region, waveguide optimization, device process, and thermal management[22, 23]. A. Wittman reported that QCL grown by MBE can operate at a record high temperature of 423 K, but its power was limited[23]. Note that the maximum temperature is only limited by our heat sink solder. Considering the melting point of indium solder is 430 K, we did not further increase the temperature to prevent the indium contact from melting. By using a gold-tin alloy with a melting point of 550 K as heat sink solder, the device has the potential to operate at much higher temperatures.

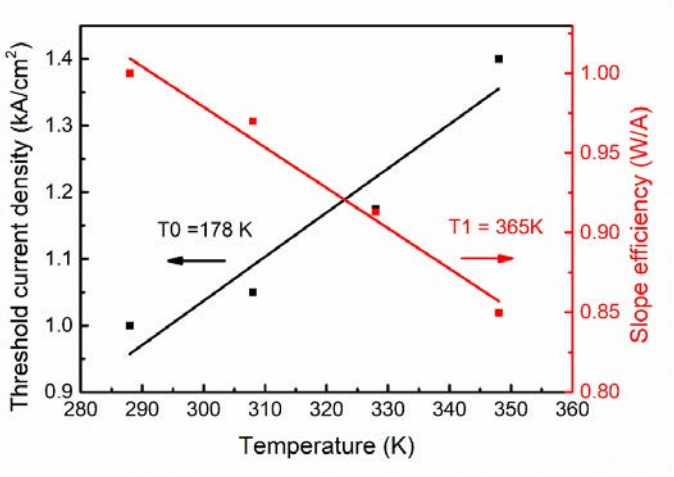

Fig. 4. Threshold current density and slope efficiency at different temperatures in pulse conditions at 1 μs, 1% duty cycle.

Fig.4 shows temperature-dependent threshold current density J_{th} and slope efficiency η in pulse mode. According to the empirical formula:

$$J_{th} = J_0 exp(T/T_0)$$

$$\eta_{slope} = \eta_0 exp(-T/T_1),$$

where T is the heat sink temperature, T_0 and T_1 are the characteristic temperature coefficient of the pulsed threshold-current density and slope efficiency. The fitting parameters are T_0 = 178 K and T_1 = 365 K. Besides the relatively low threshold current density, the T_0 of the device is comparable with the one of the highest reported CW-operating temperture QCLs[23]. As discussed by D.Botez[6], low threshold current density, high T_0 and narrow-ridge, BH devices mounted on high-thermal conductivity submounts are required to maximize the CW-operating temperature.

Combining with the above characterization of material properties, it is credible to ascribe the high performances of our QCLs to the reduced IFR. The IFR can be approximated by parameterizing the random roughness profile of the interface, i.e., the average root-mean-square height Δ and the characteristic lateral dimension Λ of the roughness. The IFR scattering rate of a QCL is given by[24]:

$$\hbar\tau_{IFR}^{-1} = \frac{\pi m^*}{\hbar^2}\Delta^2\Lambda^2\delta U^2\sum_i\{\varphi_2(z_i)\varphi_1(z_i)\}^2 e^{\frac{-\Lambda^2 q_{21}^2}{4}},$$

where m^* is the conduction band effective mass, $\hbar$ is the normalized Planck's constant, δU^2 is the the conduction band offset, $\varphi_2(z_i)$ and $\varphi_1(z_i)$ are the wavefunction amplitudes at the ith interface, q_{21} is the absolute value of the two-dimensional scattering vector. As can be seen from this expression, the IFR scattering rate is approximately proportional to the square of the IFR, i.e., $\Delta\Lambda$. The IFR plays an important role in the intersubband scattering process by reducing the lifetime of the upper state. It has been proved both theoretically and experimentally that IFR scattering is the dominant intersubband scattering mechanism for the long wavelength (>8 μm) QCLs[24]. Larger upper states lifetime and thus higher gain coefficient can be expected due to the reduced IFR, which has been confirmed by the record-narrow XRD satellite peaks. In addition, thermally activated current leakage via IFR scattering will occur when the operating temperature is high enough[25]. Therefore, the reduced IFR raises the starting point of temperature for current leakage, which results in the high operating temperature of our device.

Fig.5 (a) shows the device lasing spectrum at room temperature. Emission spectrum centering at

1175 cm^{-1} (8.5 μm) was obtained by Fourier transformed infrared spectrometer (FTIR) with a resolution of 0.25 cm^{-1} in rapid scan mode. The transverse mode is another characteristic affecting the actual application of QCLs. Fig.5 (b) shows the beam image in pulse mode operation. The fundamental transverse mode could be clearly observed by placing a pyroelectric camera 20 cm away from the collimated chip, demonstrating the device is a practical mid-infrared light source.

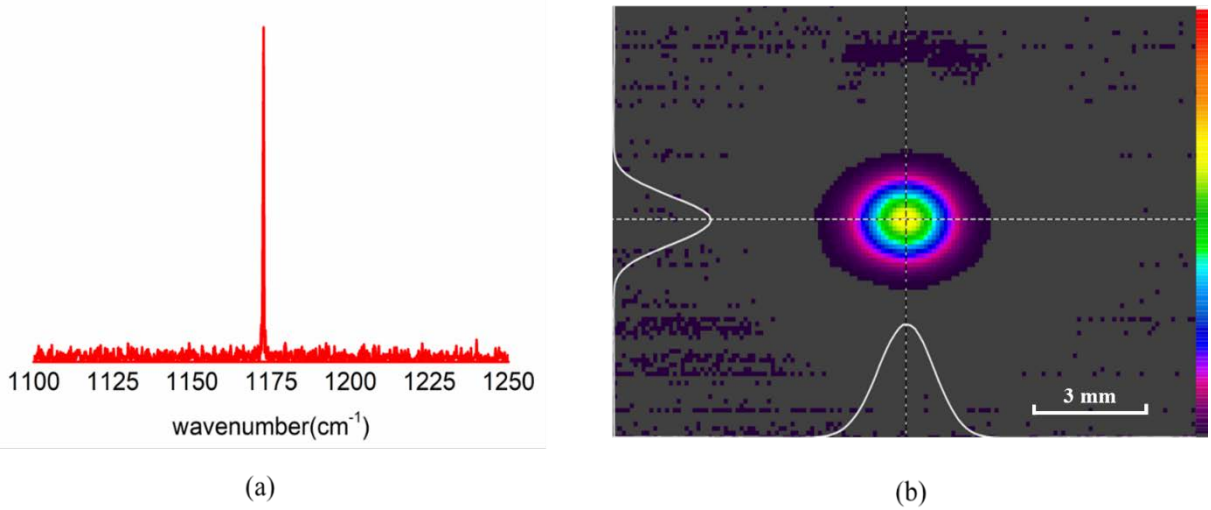

(a) (b)

Fig. 5. (a) Emission spectrum at current slightly above threshold. (b) Beam picture in pulse mode at room temperature.

4. Conclusion

In conclusion, high-performance CW operation QCL grown by MOCVD is demonstrated. High-quality interface quantum cascade structures can be realized by carefully controlling and optimizing growth conditions. The 4 mm-long, HR-coated QCL device exhibits 1.04 W CW output at 288 K at λ ~ 8.5 μm. The threshold current density and wall-plug efficiency are 1.18 kA/cm^2 and 7.1%, respectively. The device shows the capability to operate at 408 K, and the CW optical power is still 160 mW, showing a robust temperature characteristic. In addition, the fundamental transverse mode can be clearly observed. Future work should be conducted on longer devices with anti-reflective coating on the front side to reach higher CW power and WPE.

Acknowledgments

The authors would thank Ping Liang and Ying Hu for their help with device fabrication.

This work was supported by the National Key Research and Development Program of China (Grant Nos. 2020YFB0408401), in part by the National Natural Science Foundation of China (Grant Nos. 61991430, 61774146, 61790583, 61734006, 61835011, 61674144, 61774150, 61805168), in part by Beijing Municipal Science & Technology Commission (Grant No. Z201100004020006), and in part by the Key projects of the Chinese Academy of Sciences (Grant Nos. 2018147, Grant Nos. YJKYYQ20190002, Grant QYZDJ-SSW-JSC027, GrantXDB43000000, Grant ZDKYYQ20200006).

References

[1] Faist J, Capasso F, Sivco D, et al. Quantum cascade laser. Science, 1994, 264(5158), 553.
[2] Hugi A, Villares G, Blaser S, et al. Mid-infrared frequency comb based on a quantum cascade laser.

Nature, 2012, 492(7428), 229.
[3] Zhang J, Wang L, Zhang W, et al. Holographic fabricated continuous wave operation of distributed feedback quantum cascade lasers at λ ≈ 8.5 μm. Journal of Semiconductors, 2011, 32(4), 044008.
[4] Faist J, Beck M, Allen T, et al. Quantum-cascade lasers based on a bound-to-continuum transition. Applied Physics Letters, 2001, 78(2), 147.
[5] Beck M, Hofstetter D, Aellen T, et al. Continuous wave operation of a mid-infrared semiconductor laser at room temperature. Science, 2002, 295(5553), 301.
[6] Botez D, Chang C, and Mawst L J, Temperature sensitivity of the electro-optical characteristics for mid-infrared (λ = 3–16μm)-emitting quantum cascade lasers. Journal of Physics D: Applied Physics, 2016, 49(4), 043001.
[7] Wang C A, Schwarz B, Siriani D F, et al. MOVPE Growth of LWIR AlInAs/GaInAs/InP Quantum Cascade Lasers: Impact of Growth and Material Quality on Laser Performance. IEEE Journal of Selected Topics in Quantum Electronics, 2017, 23(6), 1.
[8] Feng X, Caneau C, Leblanc H P, et al. Watt-level room temperature continuous-wave operation of quantum cascade lasers with λ >10 μm. IEEE Journal of Selected Topics in Quantum Electronics, 2013, 19(4), 1200407.
[9] Wang C A, Schwarz B, Siriani D F, et al. Sensitivity of heterointerfaces on emission wavelength of quantum cascade lasers. Journal of Crystal Growth, 2017, 464, 215.
[10] Zhou W, Lu Q Y, Wu D H, et al. High-power, continuous-wave, phase-locked quantum cascade laser arrays emittin-g at 8 microm. Opt Express, 2019, 27(11), 15776.
[11] Schwarz B, Wang C A, Missaggia L, et al. Watt-level continuous-wave emission from a bifunctional quantum cascade laser/detector. ACS Photonics, 2017, 4(5), 1225.
[12] Botez D, Kirch J D, Boyle C, et al. High-efficiency, high-power mid-infrared quantum cascade lasers [Invited]. Optical Materials Express, 2018, 8(5), 1378.
[13] Lyakh A, Maulini R, Tsekoun A, et al. 3 W continuous-wave room temperature single-facet emission from quantum cascade lasers based on nonresonant extraction design approach. Applied Physics Letters, 2009, 95(14), 141113.
[14] Khurgin J B, Dikmelik Y, Liu P Q, et al. Role of interface roughness in the transport and lasing characteristics of q-uantum-cascade lasers. Applied Physics Letters, 2009, 94(9), 091101.
[15] Fujita K, Furuta S, Sugiyama A, et al. High-performance λ ~8.6 μm quantum Cascade Lasers With Single Phonon-Continuum Depopulation Structures. IEEE Journal of Quantum Electronics, 2010, 46(5), 683.
[16] Figueiredo P, Suttinger M, Go R, et al. Progress in high-power continuous-wave quantum cascade lasers [Invited]. Appl Opt, 2017, 56(31), H15.
[17] Lü X, Luna E, Schrottke L, et al. Determination of the interface parameter in terahertz quantum-cascade laser structures based on transmission electron microscopy. Applied Physics Letters, 2018, 113(17), 172101.
[18] Fewster P F. Interface roughness and period variations in MQW structures determined by X-ray diffraction. Journal of applied crystallography, 1988, 21(5), 524.
[19] Fewster, P.F., X-ray diffraction from low-dimensional structures. Semiconductor science and technology, 1993, 8(11), 1915.
[20] Savage D, Kleiner J, Schimke N, et al. Determination of roughness correlations in multilayer films for x-ray mirrors. Journal of applied physics, 1991, 69(3), 1411.
[21] Lyakh A, Maulini R, Tsekoun A, et al. Multiwatt long wavelength quantum cascade lasers based on high

strain composition with 70% injection efficiency. Optics Express, 2012, 20(22), 24272
[22] Yang P, Zhang J, Gu Z, et al. Coupled-ridge waveguide quantum cascade laser array lasing at λ ~ 5 μm. Journal of Semiconductors, 2021, 42(1), 5.
[23] Wittmann A, Bonetti Y, Fischer M, et al. Distributed-feedback quantum-cascade lasers at 9 μm operating in continuous wave up to 423 K. IEEE Photonics Technology Letters, 2009, 21(12), 814.
[24] Chiu Y, Dikmelik Y, Liu P Q, et al. Importance of interface roughness induced intersubband scattering in mid-infrared quantum cascade lasers. Applied Physics Letters, 2012, 101(17), 171117.
[25] Semtsiv M P, Flores Y, Chashnikova M, et al. Low-threshold intersubband laser based on interface-scattering-rate engineering. Applied Physics Letters, 2012, 100(16), 163502.